

Transport in line junctions of $\nu = 5/2$ quantum Hall liquids

Chenjie Wang and D. E. Feldman

Physics Department, Brown University, Providence, Rhode Island 02912, USA

(Dated: February 6, 2020)

We calculate the tunneling current through long line junctions of a $\nu = 5/2$ quantum Hall liquid and i) another $\nu = 5/2$ liquid, ii) an integer quantum Hall liquid and iii) a quantum wire. Momentum resolved tunneling provides information about the number, propagation directions and other features of the edge modes and thus helps distinguish several competing models of the $5/2$ state. We investigate transport properties for two proposed Abelian states: $K = 8$ state and 331 state, and four possible non-Abelian states: Pfaffian, edge-reconstructed Pfaffian, and two versions of the anti-Pfaffian state.

PACS numbers: 73.43.Jn, 73.43.Cd, 73.63.Nm, 73.63.Rt

I. INTRODUCTION

One of the most interesting aspects of the quantum Hall effect (QHE) is the presence of anyons which carry fractional charges and obey fractional statistics. In many quantum Hall states, elementary excitations are Abelian anyons¹. They accumulate non-trivial statistical phases when move around other anyons and can be viewed as charged particles with infinitely long solenoids attached. A more interesting theoretical possibility involves non-Abelian anyons². In contrast to Abelian QHE states, non-Abelian systems change not only their wave functions but also their quantum states when one anyon encircles another. This property makes non-Abelian anyons a promising tool for quantum information processing³.

However, their existence in nature remains an open question.

It has been proposed that non-Abelian anyons might exist in the QHE liquid at the filling factor $\nu = 5/2$, Ref. 4. Possible non-Abelian states include different versions of Pfaffian and anti-Pfaffian states^{5,6,7}. At the same time, Abelian candidate wave functions such as $K = 8$ and 331 states were also suggested^{7,8} for $\nu = 5/2$. Different models predict different quasiparticle statistics but the same quasiparticle charge $q = e/4$, where $e < 0$ is an electron charge. Since the experiments^{9,10,11} have been limited to the determination of the charge of the elementary excitations, the correct physical state remains unknown.

Several methods to probe the statistics in the $5/2$ state were suggested but neither was successfully implemented so far. This motivates further investigations of possible ways to test the statistics. The definition of exchange statistics involves quasiparticle braiding. Hence, interferometry is a natural choice. The conceptually simplest interferometry approach involves an anyonic Fabry-Perot interferometer^{12,13,14,15,16}. Its practical implementation faces difficulties due in part to the fluctuations of the trapped topological charge¹⁷. An approach based on a Mach-Zehnder interferometer^{18,19,20,21,22} is free from this limitation but just like the Fabry-Perot interferometry it cannot distinguish Pfaffian and anti-Pfaffian states. On the other hand, the structure of edge states contains full information about the bulk quantum Hall liquid and thus a tunneling experiment with a single quantum point contact might be sufficient⁷. Unfortunately, even in the case of simpler Laughlin states the theory and experiment have not been reconciled for this type of measurements²³. Besides, the scaling behavior of the tunneling $I-V$ curve is non-universal and depends on the long range Coulomb interactions. An approach based on two-point-contact geometry²⁴ identifies different states through their universal signatures in electric transport. This comes at the expense of the necessity to measure both current and noise. Recently an approach based on tunneling through a long narrow strip of the quantum Hall liquid was proposed²⁵. This approach, however, suffers from the same limitation as the Fabry-Perot geometry: in-

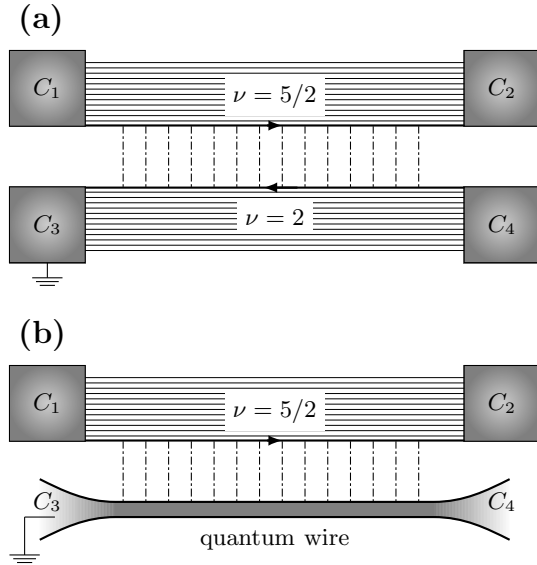


FIG. 1: (a) Tunneling between $\nu = 5/2$ and $\nu = 2$ QHE liquids. The edges of the upper and lower QHE liquids form a line junction. (b) Tunneling between $\nu = 5/2$ QHE liquid and a quantum wire. In both setups, contacts C_1 and C_2 are kept at the same voltage V .

interference is smeared by the quasiparticle tunneling into and from the strip. In this paper we analyze a related approach with tunneling through a long narrow line junction of quantum Hall liquids and a line junction of a $\nu = 5/2$ quantum Hall liquid and a quantum wire. Since only electrons tunnel in such geometry, the interference picture is not destroyed by quantum fluctuations.

Fig. 1 shows sketches of our setups. Electrons tunnel from the $\nu = 5/2$ fractional QHE state to the $\nu = 2$ integer QHE state through a line junction in the weak tunneling regime (Fig. 1(a)) at near zero temperature. A similar setup has already been realized in the integer QHE regime²⁶. Fig. 1(b) illustrates a setup with electron tunneling between the edge of the $\nu = 5/2$ liquid and a one-channel quantum wire. The most important feature in these setups is the conservation of both energy and momentum in each tunneling event^{26,27,28}. The two conservation laws lead to singularities in the $I - V$ curve. Each singularity emerges due to one of the edge modes on one side of the junction. Thus, the setup allows one to count the modes and distinguish different proposed states since they possess different numbers and types of edge modes with different propagation directions and velocities. In particular, this setup is able to distinguish different Abelian and non-Abelian states.

The paper is organized as follows. We review several models of the $5/2$ state and their corresponding edge modes in Sec. II. Sec. III contains a qualitative discussion of the momentum resolved tunneling. We describe our technical approach in Sec. IV and discuss calculations for each edge state in Sec. V. Our results are summarized in Sec. VI.

II. PROPOSED $5/2$ STATES

Although spin-unpolarized states²⁹ were suggested, numerical experiments^{30,31} support a spin-polarized state for the quantum Hall liquid with $\nu = 5/2$. Below we review the simplest spin-polarized candidate states, including the Abelian $K = 8$ and 331 states, and non-Abelian Pfaffian and Anti-Pfaffian states. In all those states, the lowest Landau level is fully filled with both spin-up and spin-down electrons which form two integer QHE liquids, while in the second Landau level electrons form a spin-polarized $\nu = 1/2$ fractional QHE liquid. In the following, we focus on the $1/2$ fractional QHE liquid and its edge. The lowest Landau level contributes two more edge channels.

The abelian $K = 8$ and 331 states⁷ are described by the Ginzburg-Landau-Chern-Simons effective theories³², with the Lagrangian density given by

$$\mathcal{L} = -\frac{\hbar}{4\pi} \sum_{IJ\mu\nu} K_{IJ} a_{I\mu} \partial_\nu a_{J\lambda} \epsilon^{\mu\nu\lambda}, \quad (1)$$

where $\mu, \nu = t, x, y$ are space-time indices. The K -matrix describes the topological orders of the bulk, and its dimension gives the number of layers in the hierarchy. The

$U(1)$ gauge field $a_{I\mu}$ describes the quasiparticle/quasihole density and current in the I th hierarchical condensate. This effective bulk theory also determines the theory at the edge, where the $U(1)$ gauge transformations are restricted. The edge theory, called chiral Luttinger liquid theory, has the Lagrangian density

$$\mathcal{L}_{\text{edge}} = -\frac{\hbar}{4\pi} \sum_{IJ} (\partial_t \phi_I K_{IJ} \partial_x \phi_J + \partial_x \phi_I V_{IJ} \partial_x \phi_J). \quad (2)$$

The chiral boson field ϕ_I describes gapless edge excitations of the I th condensate, and V_{IJ} is the interaction between the edge modes. We see that the dimension of the K -matrix gives the number of edge modes. In the $K = 8$ state, electrons first pair into charge- $2e$ bosons, then these bosons condense into a $\nu = 1/8$ Laughlin state. Hence, the K -matrix is a 1×1 matrix whose only element equals 8, and so there is only one right-moving edge mode. The 331 state is characterized by

$$K = \begin{pmatrix} 3 & -2 \\ -2 & 4 \end{pmatrix} \quad (3)$$

which has two positive eigenvalues, so there are two right-moving modes at the edge.

The Pfaffian state⁴ can be described by the following wave function for the $1/2$ fractional QHE liquid

$$\Psi_{\text{Pf}} = \text{Pf} \left(\frac{1}{z_i - z_j} \right) \prod_{i < j} (z_i - z_j)^2 e^{-\sum_i |z_i|^2}, \quad (4)$$

in which $z_n = x_n + iy_n$ is the coordinate of the n th electron in units of the magnetic length l_B , and Pf is the Pfaffian of the antisymmetric matrix $1/(z_i - z_j)$. At the edge, there is one right-moving charged boson mode and one right-moving neutral Majorana fermion mode. The edge action assumes the form (42). In the presence of edge reconstruction, the action changes⁷. In the reconstructed edge state, there are one right-moving charged and one right-moving neutral boson mode, and one left-moving neutral Majorana fermion mode. The edge action becomes Eq. (44).

The anti-Pfaffian state^{5,6} is the particle-hole conjugate of the Pfaffian state. In the absence of Landau level mixing, the $1/2$ QHE liquid system has particle-hole symmetry and thus the anti-Pfaffian state is energetically degenerate with the Pfaffian state. The wave function of the anti-Pfaffian state can be obtained through a particle-hole transformation³³, given in Ref. 5. There are two versions of the anti-Pfaffian edge states. One possibility is a non-equilibrated edge. In that case tunneling between different edge modes can be neglected and the modes do not equilibrate. The action contains two contra-propagating charged boson modes and one left-moving neutral Majorana fermion mode Eq. (52). The other version is the disorder-dominated state, in which there are one right-moving charged boson mode and three left-moving neutral Majorana fermion modes of exactly the same velocity, Eq. (51). As discussed below, only limited information about the latter state can be extracted

from the transport through a line junction since momentum does not conserve in tunneling to a disordered edge.

We see from the above discussion that different proposed edge states have different numbers and types of modes. This important information can be used to detect the nature of the $5/2$ state as discussed in the rest of this paper. It is worth to pay special attention to the Majorana fermion modes which are always neutral and do not participate in the repulsive Coulomb interaction. As a result they are slower than the charged modes.

III. QUALITATIVE DISCUSSION

In this section we discuss some details of the setup. We also provide a qualitative explanation of the results of the subsequent sections in terms of kinematic constraints imposed by the conservation laws.

Our setups are shown in Fig. 1. The long uniform junction couples the edge of the upper $\nu = 5/2$ fractional QHE liquid with the edge of the lower $\nu = 2$ integer QHE liquid. Such a system with two sides of the junction having different filling factors can be realized experimentally in semiconductor heterostructures with two mutually perpendicular 2D electron gases (2DEG)^{27,34}. Properly adjusting the direction and magnitude of the magnetic field one can get the desired filling factors²⁷. In Sec. VI, we will also briefly discuss the tunneling between two $5/2$ states. This situation can be realized by introducing a barrier in a single 2DEG²⁶. We will see however that the second setup is less informative than the first one. Finally, we will consider tunneling between a $5/2$ edge and a uniform parallel one-channel quantum wire. Below we will use the language referring to tunneling between two QHE liquids, a $5/2$ liquid and an integer QHE liquid. This language can be easily translated to the quantum wire situation. In contrast to the integer QHE edge, a quantum wire contains contra-propagating modes. However, the energy and momentum conservation, together with the Pauli principle, generally restrict tunneling to only one of those modes.

The Hamiltonian assumes the following general structure:

$$H = H_{5/2} + H_{\text{int}} + H_{\text{tun}}, \quad (5)$$

where the three contributions denote the Hamiltonians of the $5/2$ edge, the integer edge and the tunneling term. The latter term expresses as

$$H_{\text{tun}} = \int dx \psi^\dagger(x) \sum_n \Gamma_n(x) \psi_n(x) + \text{H.c.}, \quad (6)$$

where $\psi^\dagger(x)$ is the electron creation operator at the integer edge, ψ_n are electron operators at the fractional QHE edge and $\Gamma_n(x)$ are tunneling amplitudes. Several operators ψ_n correspond to different edge modes. We assume that the system is uniform. This imposes a restriction

$$\Gamma_n(x) \sim \exp(-i\Delta k_n x), \quad (7)$$

where Δk_n should be understood as the momentum mismatch between different modes. In order to derive Eq. (7) we first note that in a uniform system $|\Gamma_m(x)|$ cannot depend on the coordinate. Next, we consider the system with the tunneling Hamiltonian $H'_{\text{tun}} = \psi^\dagger(x_0)\Gamma_m(x_0)\psi_m(x_0) + \psi^\dagger(x_0+a)\Gamma_m(x_0+a)\psi_m(x_0+a) + \text{H.c.}$ The current can depend on a only and not on x_0 - otherwise different points of the junction would not be equivalent. Applying the second order perturbation theory in Γ_m to the calculation of the current one finds that $\Gamma_m(x_0)\Gamma_m^*(x_0+a)$ must be a constant, independent of x_0 . Using the limit of small a one now easily sees that the phase of the complex number $\Gamma_m(x)$ is a linear function of x . This proves Eq. (7).

We assume that the same voltage V is applied to both contacts at the upper $\nu = 5/2$ edge in Fig. 1, so that all right-moving and left-moving modes at the upper edge are in equilibrium with the chemical potential $\mu_1 = eV$. The lower edge is grounded, i.e., the chemical potential at the lower edge $\mu_2 = 0$.

Δk_n may depend on the applied voltage V since the width of the line junction may change when the applied voltage changes. We will neglect that dependence in the case of the setup with the tunneling between two QHE liquids; more specifically, we will assume that both liquids are kept at a constant charge density and the tunneling between them is weak. In the case of the tunneling between a QHE liquid and a quantum wire we will assume that the charge density is kept constant in 2DEG but can be controlled by the gate voltage in the one-dimensional wire. The Fermi-momentum k_F in the quantum wire depends on the charged density and any change of k_F results in an equal change of all Δk_n . Thus, we will assume a setup with two 2DEG in the discussion of the voltage dependence of the tunneling current at fixed Δk_n . The setup with a quantum wire will be assumed in the discussion of the dependence of the current on k_F at a fixed low voltage. In all cases we will assume that the temperature is low.

In our calculations we will use the Luttinger liquid model for the edge states³⁵. It assumes a linear spectrum for each mode and neglects tunneling between different modes on the same edge. These assumptions are justified in the regime of low energy and momentum. Thus, we expect that the results for the tunneling between two 2DEG are only qualitatively valid at high voltage.

Our main assumption is that both energy and momentum conserve in each tunneling event. This means that we neglect disorder at the edges. This assumption needs a clarification in the case of the disorder-dominated anti-Pfaffian state because its formation requires edge disorder. We will assume that for that state only neutral modes couple to disorder and one can neglect disorder effects on the charged mode. For completeness, we include a discussion of the momentum resolved tunneling into the nonequilibrated anti-Pfaffian state. However, a much simpler experiment is sufficient to detect that state. One just needs to measure the conductance of

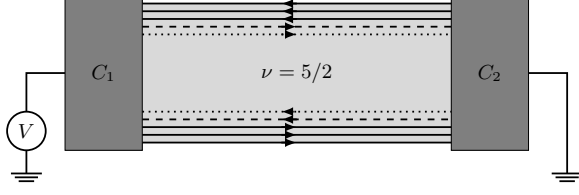


FIG. 2: A bar geometry that can be used to detect the nonequilibrated anti-Pfaffian state. Solid lines denote Integer QHE edge modes, the dashed lines denote fractional QHE charged modes and dotted lines denote Majorana modes. Arrows show mode propagation directions.

the $5/2$ -liquid in the bar geometry illustrated in Fig. 2. Indeed, in the nonequilibrated anti-Pfaffian state, disorder is irrelevant. Each nonequilibrated edge has three charged Fermi-liquid modes propagating in one direction and another Luttinger-liquid charged mode (and a neutral mode) propagating in the opposite direction. In the bar geometry, the lower edge carries the current $3e^2V/h$. The upper charged mode carries the current $e^2V/(2h)$ in the same direction. Hence, the total current is $7e^2V/(2h)$ and the conductance is $7/2$ and not $5/2$ conductance quanta. Our discussion assumes an ideal situation with no disorder. In a large system even weak disorder, irrelevant in the renormalization group sense, might result in edge equilibration. Nevertheless, if the QHE bar is shorter than the equilibration length the nature of the state can be probed by the conductance measurement in the bar geometry.

Before presenting the calculations we will discuss a qualitative picture. Unless otherwise specified we consider $\Delta k_n > 0$. As seen from the calculations in the following section, the particle-hole symmetry for Luttinger liquids implies that the tunneling current at negative Δk_n can be found from the relation $I_{\text{tun}}(V, \Delta k) = -I_{\text{tun}}(-V, -\Delta k)$.

At the lower edge there are two edge modes for spin-up and -down electrons. At the upper edge there are two spin-up and -down integer modes and one or more modes corresponding to the $\nu = 1/2$ edge. Spin is conserved during the tunneling process. Thus we have three contributions to the tunneling current: (A) tunneling between the upper spin-down fractional edge modes and the lower spin-down integer edge mode; (B) tunneling between the upper spin-down integer edge mode and the lower spin-down integer edge mode; (C) tunneling between the upper spin-up integer edge mode and the lower spin-up integer edge mode. We use only the lowest order perturbation approximation so these contributions are independent. Thus, the total tunneling current is $I_{\text{tun}} = I_{\text{tun}}^A + I_{\text{tun}}^B + I_{\text{tun}}^C$. Contributions (B) and (C) are similar since the Zeeman energy is small compared to Coulomb interactions under typical magnetic fields.

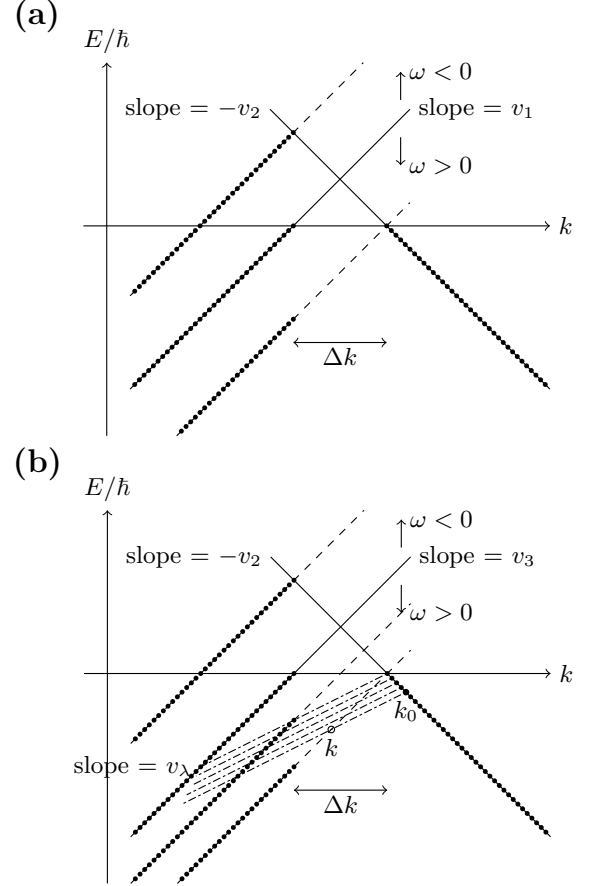


FIG. 3: Illustration of the graphical method. (a) Tunneling between two integer QHE modes. The left solid line represents the electron spectrum at the upper edge at zero voltage. The right solid line represents the spectrum at the lower edge. The dashed lines represent the electron spectra at the upper edge at different voltages. Black dots represent occupied states. The momentum mismatch between two edges $\Delta k > 0$. (b) Tunneling between an integer QHE edge and a Pfaffian edge. The right line represents the spectrum of the integer edge. The left line shows the spectrum of the charged boson mode at the Pfaffian edge. The unevenly dashed lines (λ lines) represent Majorana fermions. The figure illustrates a tunneling event in which an electron with the momentum k_0 tunnels into the Pfaffian edge and creates a boson with the momentum k and a Majorana fermion with the momentum $k_0 - k$.

Thus, we will only consider spin-down electrons below.

All edge modes are chiral Luttinger liquids with the spectra of the form $E = \pm v_\alpha(k - k_{F\alpha})$, where $\pm v_\alpha$ is the edge mode velocity, the sign reflects the propagation direction. We will first consider case (B) (case (C) is identical), tunneling between two integer Fermi-liquid edge modes. Denote the upper edge velocity as v_1 and the lower edge velocity as v_2 . If an electron of momentum k from the upper edge tunnels into the lower edge

or vice versa, energy and momentum conservation gives

$$v_1(k - k_{F1}) - \omega = -v_2(k - k_{F2}), \quad (8)$$

where $\omega = -eV/\hbar$ (in the rest of this paper, we will refer to both ω and V as the applied voltage). The tunneling happens only when $(k - k_{F1})(k - k_{F2}) < 0$, i.e., one of the two states is occupied and the other is not. Eq. (8) is easy to solve directly but a graphical approach is more transparent. Fig. 3(a) shows the spectra in the energy-momentum space, where the left line describes the upper edge mode and the right line describes the lower edge mode, and the intersection point represents the solution of Eq. (8). The black dots represent occupied states. We see that when $\omega = 0$, both states in the intersection point are unoccupied, therefore no tunneling happens. When ω increases, the left line moves down. For a small ω , there is still no tunneling. After ω reaches the value of $v_1\Delta k = v_1(k_{F2} - k_{F1})$ and the state from the right line on the intersection point becomes occupied, an electron from the lower edge can tunnel into the upper edge. This results in a positive contribution to the tunneling current. Since the tunneling happens only at the intersection point and the tunneling density of states (TDOS) is a constant in Fermi liquids, the current will remain constant for $\omega > v_1\Delta k$. For a negative ω , the situation is similar. Before ω reaches the value $-v_2\Delta k$, i.e., $|\omega| < v_2\Delta k$, no tunneling happens. When $|\omega| > v_2\Delta k$, an electron from the upper edge can tunnel into the lower edge and a negative voltage-independent tunneling current results. Thus, the $I_{\text{tun}}^B - V$ characteristics is a sum of two step functions, with two jumps at $\omega = -v_2\Delta k$ and $v_1\Delta k$. The positions of the two jumps provide the information about the edge mode velocities. The differential conductance G_{tun}^B is simply a combination of two δ -functions of ω .

This graphical method can also be used to analyze Case (A). Consider the $K = 8$ state as the simplest example. For the $K = 8$ state, only electron pairs can tunnel through the junction since single electrons are gapped. This does not create much difference for the further analysis. It is convenient to use bosonization language for the description of the $K = 8$ edge. All elementary excitations are bosons with positive momenta $k - k_{F2} > 0$ and linear spectrum. Thus, the relation between the momentum and energy remains the same as in the Fermi liquid case. Hence, the $I_{\text{tun}}^A - V$ curve has singularities at $\omega = -v_2\Delta k$ and $\omega = v_3\Delta k$, where v_3 is the velocity at the $K = 8$ fractional edge. However, the current is no longer a constant above the thresholds because of a different TDOS. We will see below that the current exhibits universal power-law dependence on the voltage bias near the thresholds.

In the Pfaffian state, case (A) involves three modes: a charged boson mode ϕ_3 and a neutral Majorana fermion mode λ from the upper edge, and the Fermi-liquid mode from the lower edge. They have velocities v_3 , v_λ and v_2 respectively. Any tunneling event involves creation of a Majorana fermion. The spectrum of the Majorana

mode is linear: $E = v_\lambda k > 0$. The total energy and momentum of the three modes should be conserved. As usual, we denote the momentum mismatch between the upper and lower edges as Δk . Fig. 3(b) demonstrates the graphical approach for the Pfaffian state. The left line represents the spectrum of the charged boson at the upper edge and the right line describes the spectrum of the lower edge. Consider a tunneling process such that an electron from the lower edge tunnels into the upper edge. This may happen at a positive applied voltage. In this process the electron emits a Majorana fermion and creates excitations of the charged boson mode at the upper edge. The energy and momentum of the electron are the sums of the energies and momenta of the charged boson and Majorana modes. The unevenly dashed lines of slope v_λ in Fig. 3(b) represent the Majorana fermion. We will call them λ -lines. Different λ -lines start at different *occupied* states on the right line and correspond to different momenta of the electron at the lower edge. One can visualize the tunneling process in the following way: an electron with the momentum k_0 from the right line slides along the λ -line (emitting a Majorana fermion with the momentum $k_0 - k$) and reaches the left line at $k > k_{F3}$ (otherwise the tunneling is not possible since the momentum change $(k - k_{F3})$ of the Bose mode must be positive). Both energy and momentum are conserved in such picture. Because the Majorana fermion has a positive momentum the λ -line points downward and leftward. When ω is positive and small enough, all the states at the intersections of the left line with the λ -lines have $k < k_{F3}$, thus, no tunneling happens. At $\omega = v_\lambda\Delta k$, the highest λ -line intersects the left line at $k = k_{F3}$, so the tunneling becomes possible and contributes a positive current. Thus $\omega = v_\lambda\Delta k$ is the positive threshold voltage. When ω reaches $v_3\Delta k$, the intersection point of the right and left lines corresponds to $k > k_{F3}$ (an ‘empty state’) at the upper edge and a filled state at the lower edge. The tunneling process involving those two states and a zero-momentum Majorana fermion becomes possible. This results in another singularity in the $I_{\text{tun}}^A - V$ curve. For negative ω , it is expected that a Majorana fermion and an excitation of the charged boson mode combine into an electron and tunnel into the lower edge. The same analysis as above shows that there is no current when ω is negative and small. When $\omega = -v_2\Delta k$, the tunneling process involving a zero-momentum Majorana fermion becomes possible. Thus, $\omega = -v_2\Delta k$ is the negative threshold voltage in the $I_{\text{tun}}^A - V$ curve. We see three singularities in the tunneling current in agreement with the presence of three modes.

For all other proposed fractional states, the graphical method also works but becomes more complicated, so we will not discuss them in detail here. The above discussion, based only on the conservation of energy and momentum, confirms that singularities appear in the $I_{\text{tun}}^A - V$ characteristics and they are closely related to the number and nature of the edge modes. In the following section, we discuss the calculations based on the

chiral Luttinger liquid theory.

The calculations below involve the velocities of the charged and neutral edge modes. We generally expect charged modes to be faster. Indeed, in the chiral Luttinger liquid theory the kinetic energy and the Coulomb interaction enter in the same form, quadratic in the Bose-fields. Since the Coulomb contribution exists only for the charged mode, it is expected to have a greater velocity.

IV. CALCULATION OF THE CURRENT

We now calculate the tunneling current. In this section we derive a general expression, valid for all models. In the next section it will be applied to the six models discussed above.

As mentioned above, to the lowest order of the perturbation theory the tunneling current can be separated into three independent parts, $I_{\text{tun}} = I_{\text{tun}}^A + I_{\text{tun}}^B + I_{\text{tun}}^C$. The calculation of I_B and I_C is essentially the same. So in the following, we will only consider I_{tun}^A and I_{tun}^B .

We will use below the bosonization language which can be conveniently applied to all modes except Majorana fermions. Thus, we will not explicitly discuss Majorana modes in this section. However, all results can be extended to the situation involving Majorana fermions without any difficulty. Indeed, in the lowest order of the perturbation theory only the two-point correlation function of the Majorana fermion operators is needed. It is the same as for ordinary fermions and the case of ordinary fermions can be easily treated with bosonization.

We consider the Lagrangian density³⁵

$$\begin{aligned} \mathcal{L} = & \mathcal{L}_{\text{frac}}(t, x) - \frac{1}{4\pi} \partial_x \phi_1 (\partial_t + v_1 \partial_x) \phi_1 \\ & - \frac{1}{4\pi} \partial_x \phi_2 (-\partial_t + v_2 \partial_x) \phi_2 - \mathcal{H}_{\text{tun}}, \end{aligned} \quad (9)$$

with tunneling Hamiltonian density

$$\mathcal{H}_{\text{tun}} = \sum_n \gamma_A^n \Psi_2^\dagger(x) \Psi_{\text{frac}}^n(x) + \gamma_B \Psi_2^\dagger(x) \Psi_1(x) + \text{H.c.}, \quad (10)$$

where Ψ_1 is the electron operator for the integer QHE mode of the upper edge, Ψ_{frac}^n annihilate electrons at the 1/2-edge, Ψ_2 is the electron operator at the lower edge; Bose-fields $\phi_j(x)$ ($j = 1, 2$) represent the right/left-moving integer edge modes of velocities v_j at the upper/lower QHE liquid. The Bose-fields satisfy the commutation relation $[\phi_i(x), \phi_j(x')] = i\sigma_j \pi \delta_{ij} \text{sign}(x - x')$, with $\sigma_1 = +1$ and $\sigma_2 = -1$. The Lagrangian density for the fractional QHE edge $\mathcal{L}_{\text{frac}}$ depends on the state and will be discussed in detail later. Coulomb interactions within the fractional edge (between different modes) will be considered but the interactions between different edges and between fractional and integer QHE edge modes of the 5/2 liquid are neglected in our model. The inter-edge interactions, presumably weaker than the

intra-edge interactions, are assumed to affect our quantitative results only but will not change our qualitative picture.

We assume that the line junction is infinitely long and the system is spatially uniform. As discussed above this restricts possible coordinate dependence of the tunneling amplitudes. It will be convenient for us to assume that γ_A^n and γ_B are independent of the coordinate and absorb the factors $\exp(-i\Delta k_n x)$ into the electron creation and annihilation operators. The tunneling amplitudes are also assumed to be independent of the applied voltage V . In the tunneling Hamiltonian density (10), $\Psi_j(x)$ is the corresponding electron operator of the integer mode $\phi_j(x)$ with $\Psi_j = e^{\sigma_j i \phi_j + i k_{F,j} x}$, where $k_{F,j}$ represents the Fermi momentum. The corresponding electron density $\rho_j = \partial_x \phi_j / 2\pi$. In the fractional edge, there may be several relevant electron operators Ψ_{frac}^n . In our calculations, only the most relevant electron operators will be considered, in the sense of the renormalization group theory. Usually, tunneling between integer QHE modes is more relevant than tunneling into the fractional $\nu = 1/2$ edge mode. However, as is clear from the above discussion, the tunneling conductance $G_{\text{tun}}^B(\omega)$ is just a combination of two δ -functions, therefore the shape of the voltage dependence of the total differential conductance G_{tun} is determined by $G_{\text{tun}}^A(\omega)$.

Since the upper and lower edges have different chemical potentials, it is convenient to switch to the interaction representation with $\Psi_{\text{frac}}^n \rightarrow \Psi_{\text{frac}}^n e^{-i\mu_1 t/\hbar}$, $\Psi_1 \rightarrow \Psi_1 e^{-i\mu_1 t/\hbar}$ and $\Psi_2 \rightarrow \Psi_2 e^{-i\mu_2 t/\hbar}$, where $\mu_1 = eV$ and $\mu_2 = 0$. This introduces time-dependence into the tunneling operators (cf. Ref. 36). The electron operator $\Psi_{\text{frac}}^n(x)$ can be written in a bosonized form according to the chiral Luttinger liquid theory, $\Psi_{\text{frac}}^n(x) = e^{i \sum_I (l_I \phi_I + l_I k_{F,I} x)}$, or $\lambda(x) e^{i \sum_I (l_I \phi_I + l_I k_{F,I} x)}$, if a Majorana mode $\lambda(x)$ exists. The set of integers $\{l_I\}$ satisfies certain conditions so that the electron operators anticommute with each other. In order to pay special attentions to the momentum mismatches, we define

$$\Psi_{\text{frac}}^n(x) \equiv \tilde{\Psi}_{\text{frac}}^n(x) e^{i \sum_I l_I k_{F,I} x}. \quad (11)$$

Similar definitions are also made for the integer QHE modes, $\Psi_j(x) = e^{i k_{F,j} x} \tilde{\Psi}_j(x)$. Thus, the density of tunneling Hamiltonian can be rewritten in the interaction picture as

$$\begin{aligned} \mathcal{H}_{\text{tun}} = & \sum_n \gamma_A^n e^{i\omega t - i\Delta k_{2f}^n x} \tilde{\Psi}_2^\dagger(x) \tilde{\Psi}_{\text{frac}}^n(x) \\ & + \gamma_B e^{i\omega t - i\Delta k_{21} x} \tilde{\Psi}_2^\dagger(x) \tilde{\Psi}_1(x) + \text{H.c.}, \end{aligned} \quad (12)$$

where $\Delta k_{2f}^n = k_{F,2} - \sum_I l_I k_{F,I}$, $\Delta k_{21} = k_{F,2} - k_{F,1}$ and $\omega = (\mu_2 - \mu_1)/\hbar = -eV/\hbar$. It is worth to mention that in the $K = 8$ state, electron pairs and not electrons tunnel through the junction, thus in the first term of Eq. (12) ω should be doubled because the pair charge doubles, and $\tilde{\Psi}_{\text{frac}}^n$ and $\tilde{\Psi}_2$ should be understood as bosonic operators that annihilate electron pairs.

The operator for the tunneling current density is given by,

$$j(t, x) = e \frac{d\rho_2}{dt} = \frac{e}{i\hbar} [\rho_2(x), H_{\text{tun}}], \quad (13)$$

where $\rho_2(x)$ is the electron density of the lower edge, and $H_{\text{tun}} = \int dx \mathcal{H}_{\text{tun}}(x)$ is the tunneling Hamiltonian. Expanding the commutator in Eq. (13) we get

$$j(t, x) = \frac{e}{i\hbar} \left\{ \sum_n \gamma_A^n e^{i\omega t - i\Delta k_{2f} x} \tilde{\Psi}_2^\dagger(x) \tilde{\Psi}_{\text{frac}}^n(x) + \gamma_B e^{i\omega t - i\Delta k_{21} x} \tilde{\Psi}_2^\dagger(x) \tilde{\Psi}_1(x) - \text{H.c.} \right\}. \quad (14)$$

The current can now be calculated with the Keldysh technique. We assume that the tunneling was zero at $t = -\infty$ and then gradually turned on. Both edges were in their ground states at $t = -\infty$. At zero temperature, the current is given by the expression

$$I_{\text{tun}}(t) = \langle 0 | S(-\infty, t) I S(t, -\infty) | 0 \rangle, \quad (15)$$

where $\langle 0 |$ is the initial state, the operator $I = \int dx j(t, x)$ and

$$S(t, -\infty) = T \exp(-i \int_{-\infty}^t H dt' / \hbar)$$

is the evolution operator. To the lowest order in the tunneling amplitudes, the tunneling current reduces to

$$I_{\text{tun}}(t) = -\frac{i}{\hbar} \int dx dx' \int_{-\infty}^t dt' \langle 0 | [j(t, x), \mathcal{H}_{\text{tun}}(t', x')] | 0 \rangle. \quad (16)$$

After a substitution of Eqs. (12) and (14) into Eq. (16), we can compute the tunneling current since we know all the electron correlation functions from the chiral Luttinger liquid theory.

In the lowest order perturbation theory the current does not contain any cross-terms, proportional to $\gamma_A^i \times (\gamma_A^j)^*$ with $i \neq j$, or $\gamma_A^i \times \gamma_B^*$. There are only contributions proportional to $|\gamma_A^i|^2$ or $|\gamma_B|^2$. Thus, without loss of generality we can assume that only one of the tunneling amplitudes is nonzero and write

$$j_{\alpha\beta}(t, x) = \frac{e}{i\hbar} (\gamma e^{i\omega t - i\Delta k x} \tilde{\Psi}_\alpha^\dagger(t, x) \tilde{\Psi}_\beta(t, x) - \text{H.c.}). \quad (17)$$

The operators $\tilde{\Psi}_\alpha$ and $\tilde{\Psi}_\beta$ represent electron operators on two sides of the junction. For the momentum mismatch Δk and tunneling amplitude γ , we have dropped their subscripts for brevity. Using Eq. (16), the tunneling current can be expressed as

$$I_{\text{tun}}^{\alpha\beta} = -\frac{e|\gamma|^2}{\hbar^2} \int dx dx' \int_{-\infty}^t dt' (e^{i\omega \Delta t - i\Delta k \Delta x} - \text{c.c.}) \times [G_{\alpha\beta}(\Delta t, \Delta x) - G_{\alpha\beta}(-\Delta t, -\Delta x)], \quad (18)$$

with $\Delta t = t - t'$, $\Delta x = x - x'$ and

$$G_{\alpha\beta}(\Delta t, \Delta x) = \langle 0 | \tilde{\Psi}_\alpha^\dagger(t, x) \tilde{\Psi}_\alpha(t', x') \tilde{\Psi}_\beta(t, x) \tilde{\Psi}_\beta^\dagger(t', x') | 0 \rangle, \quad (19)$$

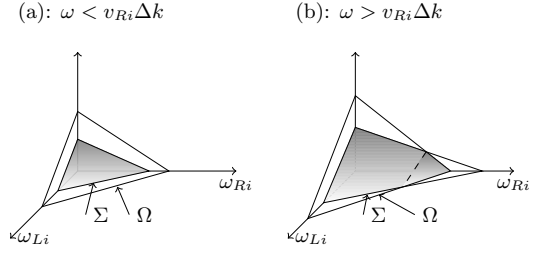


FIG. 4: A 3-dimensional illustration of the integration volume in the integral (24). The integral (24) is taken over the volume under the shaded surface in the positive orthant. In panel (a), $\omega < v_{Ri} \Delta k$ and the ω_{Ri} axis intersects superplane Σ closer to the origin than the plane Ω . In panel (b) $\omega > v_{Ri} \Delta k$ and the order of the intersection points reverses.

and we used the fact that $\langle 0 | \tilde{\Psi}_{\alpha/\beta}^\dagger(t, x) \tilde{\Psi}_{\alpha/\beta}(t', x') | 0 \rangle = \langle 0 | \tilde{\Psi}_{\alpha/\beta}(t, x) \tilde{\Psi}_{\alpha/\beta}^\dagger(t', x') | 0 \rangle$ and the translational invariance for chiral Luttinger liquids. Eq. (18) can be simplified as

$$I_{\text{tun}}^{\alpha\beta} = -L \frac{e|\gamma|^2}{\hbar^2} \int dy d\tau (e^{i\omega \tau - i\Delta k y} - \text{c.c.}) G_{\alpha\beta}(\tau, y), \quad (20)$$

where L is the length of the junction.

Let there be N right-moving and M left-moving modes in total at both edges. In the chiral Luttinger liquid theory a general expression for the correlation function is

$$G_{\alpha\beta}(\tau, y) = l_B^2 \prod_{i=1}^N \left(\frac{\tau_c}{\delta + i(\tau - y/v_{Ri})} \right)^{g_{Ri}} \times \prod_{i=1}^M \left(\frac{\tau_c}{\delta + i(\tau + y/v_{Li})} \right)^{g_{Li}}, \quad (21)$$

where v_{Ri} and v_{Li} denote the velocities of the i th right- and left-moving modes, τ_c is the ultraviolet cutoff and l_B is the magnetic length. This expression relies on the fact that the quadratic Luttinger liquid action can always be diagonalized and represented as the sum of the actions of non-interacting chiral modes. All the velocities v_{Ri}/v_{Li} and scaling exponents g_{Ri}/g_{Li} depend on the details of the Hamiltonian and this dependence is discussed separately for each state in Sec. V. We choose the convention that $v_{R1} < v_{R2} < \dots < v_{RN}$ and $v_{L1} < v_{L2} < \dots < v_{LM}$. The scaling dimension of the tunneling operator $\tilde{\Psi}_\alpha^\dagger(t, x) \tilde{\Psi}_\beta(t, x)$ is $g = 1/2(\sum_i g_{Ri} + \sum_i g_{Li})$.

Using the Fourier transformation

$$\frac{1}{(\delta + it)^g} = \int_{-\infty}^{+\infty} d\omega e^{-i\omega t} \frac{|\omega|^{g-1}}{\Gamma(g)} \theta(\omega), \quad (22)$$

we integrate out τ and y in Eq. (20). Then we obtain

$$I_{\text{tun}}^{\alpha\beta} = -4\pi^2 L \frac{e|\gamma|^2}{\hbar^2} \int [d\omega_{Ri} d\omega_{Li}] \times \left\{ \delta(\omega - \sum \omega_{Ri} - \sum \omega_{Li}) \delta(\Delta k - \sum \frac{\omega_{Ri}}{v_{Ri}} + \sum \frac{\omega_{Li}}{v_{Li}}) - (\omega \leftrightarrow -\omega, \Delta k \leftrightarrow -\Delta k) \right\} \times \prod |\omega_{Ri}|^{g_{Ri}-1} \frac{\theta(\omega_{Ri})}{\Gamma(g_{Ri})} \prod |\omega_{Li}|^{g_{Li}-1} \frac{\theta(\omega_{Li})}{\Gamma(g_{Li})}, \quad (23)$$

where we absorbed the cutoff τ_c and the magnetic length l_B into the tunneling amplitude γ for brevity. The two δ -functions represent the energy and momentum conservation. Integrating out ω_{R1} and ω_{L1} by using the two δ -functions we obtain our general expression for the tunneling current,

$$I_{\text{tun}}^{\alpha\beta} = A \int_0^\infty [d\omega_{Ri} d\omega_{Li}]_{i \geq 2} \prod_{i \geq 2} |\omega_{Ri}|^{g_{Ri}-1} \prod_{i \geq 2} |\omega_{Li}|^{g_{Li}-1} \times \left| \frac{\omega}{v_{R1}} - \Delta k - \sum_{i \geq 2} \frac{\omega_{Ri}}{v_{i1}^{RR}} - \sum_{i \geq 2} \frac{\omega_{Li}}{v_{i1}^{LR}} \right|^{g_{L1}-1} \times \theta\left(\frac{\omega}{v_{R1}} - \Delta k - \sum_{i \geq 2} \frac{\omega_{Ri}}{v_{i1}^{RR}} - \sum_{i \geq 2} \frac{\omega_{Li}}{v_{i1}^{LR}}\right) \times \left| \frac{\omega}{v_{L1}} + \Delta k - \sum_{i \geq 2} \frac{\omega_{Ri}}{v_{i1}^{RL}} - \sum_{i \geq 2} \frac{\omega_{Li}}{v_{i1}^{LL}} \right|^{g_{R1}-1} \times \theta\left(\frac{\omega}{v_{L1}} + \Delta k - \sum_{i \geq 2} \frac{\omega_{Ri}}{v_{i1}^{RL}} - \sum_{i \geq 2} \frac{\omega_{Li}}{v_{i1}^{LL}}\right) - (\omega \leftrightarrow -\omega, \Delta k \leftrightarrow -\Delta k), \quad (24)$$

with

$$A = -L \frac{4\pi^2 e|\gamma|^2}{\hbar^2 \prod \Gamma(g_{Ri}) \Gamma(g_{Li})} (v_{i1}^{RL})^{g_{R1}+g_{L1}-1} \quad (25)$$

$$v_{i1}^{RR} = \frac{v_{Ri} v_{R1}}{v_{Ri} - v_{R1}}, \quad v_{i1}^{LL} = \frac{v_{Li} v_{L1}}{v_{Li} - v_{L1}}, \quad i \geq 2, \quad (26)$$

$$v_{i1}^{RL} = \frac{v_{Ri} v_{L1}}{v_{Ri} + v_{L1}}, \quad v_{i1}^{LR} = \frac{v_{Li} v_{R1}}{v_{Li} + v_{R1}}, \quad i \geq 1. \quad (27)$$

Let us discuss the above expression in general before applying it to the six models. We first consider $\omega > 0$. In that case only the first term in Eq. (24) contributes to $I_{\text{tun}}^{\alpha\beta}$. The integration is taken over the volume in the positive orthant of the $(M+N-2)$ -dimensional space spanned by $\{\omega_{Ri}, \omega_{Li}\}_{i \geq 2}$ under both of the following superplanes

$$\Sigma: \sum_{i \geq 2} \frac{\omega_{Ri}}{v_{i1}^{RR}} + \sum_{i \geq 2} \frac{\omega_{Li}}{v_{i1}^{LR}} = \frac{\omega}{v_{R1}} - \Delta k, \quad (28)$$

$$\Omega: \sum_{i \geq 2} \frac{\omega_{Ri}}{v_{i1}^{RL}} + \sum_{i \geq 2} \frac{\omega_{Li}}{v_{i1}^{LL}} = \frac{\omega}{v_{L1}} + \Delta k. \quad (29)$$

If $\omega < v_{R1} \Delta k$ then the integration volume is 0 and so is the tunneling current. The tunneling only appears when $\omega > v_{R1} \Delta k$, thus, we see that $v_{R1} \Delta k$ is the positive

threshold voltage. It is easy to see that the asymptotic behavior of the tunneling current at $\omega \gtrsim v_{R1} \Delta k$ is

$$I_{\text{tun}}^{\alpha\beta} \sim \left(\frac{\omega}{v_{R1}} - \Delta k \right)^{\sum_{i=2}^N g_{Ri} + \sum_{i=1}^M g_{Li} - 1}. \quad (30)$$

Now let us consider the ω_{Ri} -intercepts of the two superplanes, $\Sigma_{Ri} = (\omega/v_{R1} - \Delta k) v_{i1}^{RR}$ and $\Omega_{Ri} = (\omega/v_{L1} + \Delta k) v_{i1}^{RL}$, $i \geq 2$. We find that

$$\begin{aligned} \Sigma_{Ri} &< \Omega_{Ri}, & \text{when } \omega < v_{Ri} \Delta k; \\ \Sigma_{Ri} &> \Omega_{Ri}, & \text{when } \omega > v_{Ri} \Delta k. \end{aligned} \quad (31)$$

Thus, when ω passes $v_{Ri} \Delta k$, the shape of the $(M+N-2)$ -dimensional integration volume changes, as is illustrated in Fig. 4 for the 3D case. This volume change leads to a singularity in the $I_{\text{tun}} - V$ curve. The precise nature of the singularities depends on the model and will be discussed in the following section. For the ω_{Li} -intercepts, $\Sigma_{Li} = (\omega/v_{R1} - \Delta k) v_{i1}^{LR}$ is always smaller than $\Omega_{Li} = (\omega/v_{L1} + \Delta k) v_{i1}^{LL}$, so no extra singularities emerge. Thus, we see that on the positive voltage branch, the tunneling current has N singularities in one to one correspondence with the right-moving modes.

Similar behavior of $I_{\text{tun}}^{\alpha\beta}(\omega)$ manifests itself when $\omega < 0$, with singularities at $\omega = -v_{Li} \Delta k$. Thus, each mode contributes a singularity.

V. RESULTS FOR EACH MODEL

Now using the general expression, Eq. (24), we discuss the properties of I_{tun} and G_{tun} in detail. First, let us consider the simplest case, tunneling between two integer edge modes. Following Eq. (24), it is easy to derive that

$$I_{\text{tun}}^B = -L \frac{4\pi^2 e|\gamma_B|^2 v_1 v_2}{\hbar^2 (v_1 + v_2)} \times [\theta(\omega - v_1 \Delta k_{21}) - \theta(-\omega - v_2 \Delta k_{21})]. \quad (32)$$

where v_1 and v_2 are velocities of the upper and lower edge modes respectively, Δk_{21} is the momentum mismatch between the two modes. As expected from the qualitative picture, I_{tun}^B is indeed a combination of two step functions and so G_{tun}^B is just a combination of two δ -functions. The two singularities, positive and negative thresholds, appear at $\omega = v_1 \Delta k_{21}$ and $-v_2 \Delta k_{21}$.

In the following subsections, we will discuss I_{tun}^A and G_{tun}^A as functions of both voltage ω and momentum mismatch Δk for six proposed fractional QHE states.

A. $K = 8$ state

In the fractional edge of the $K = 8$ state⁷, there is one right-moving boson mode ϕ_3 with the Lagrangian density

$$\mathcal{L}_{\text{frac}} = -\frac{2\hbar}{\pi} \partial_x \phi_3 (\partial_t + v_3 \partial_x) \phi_3. \quad (33)$$

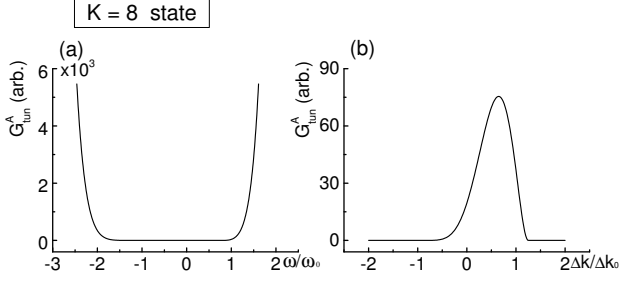


FIG. 5: (a) Voltage dependence of the differential conductance in the $K = 8$ state, at a fixed momentum mismatch Δk . Only the contribution G^A_{tun} is shown. Voltage is shown in units of $\omega_0 = v_2 \Delta k$, and the conductance is shown in arbitrary units. (b) Momentum mismatch dependence of G^A_{tun} at a fixed voltage. $\Delta k_0 = \omega/v_2$. For both curves, we set $v_3/v_2 = 0.8$.

Only electron pairs are allowed to tunnel into the edge. The electron pair annihilation operator is $\tilde{\Psi}_{\text{frac}} = e^{i8\phi_3}$, and the charge density $\rho_{\text{frac}} = e\partial_x \phi_3/\pi$. The pair correlation function is $\langle 0|\tilde{\Psi}_{\text{frac}}^\dagger(t, x)\tilde{\Psi}_{\text{frac}}(0, 0)|0\rangle = 1/[\delta + i(t - x/v_3)]^8$, i.e., the scaling exponent $g_3 = 8$. In the integer edge, Ψ_2 should also be understood as the pair annihilation operator with $\langle 0|\tilde{\Psi}_2^\dagger(t, x)\tilde{\Psi}_2(0, 0)|0\rangle = 1/[\delta + i(t + x/v_2)]^4$ and $g_2 = 4$. Substituting the scaling exponents and edge velocities into Eq. (24), we obtain

$$I_{\text{tun}}^A = -L \frac{8\pi^2 e |\gamma_A|^2}{\hbar^2 \Gamma(8) \Gamma(4)} \left(\frac{v_2 v_3}{v_2 + v_3} \right)^{11} \left(\frac{\omega}{v_3} - \Delta k_{2f} \right)^3 \left(\frac{\omega}{v_2} + \Delta k_{2f} \right)^7 \left[\theta(\omega - v_3 \Delta k_{2f}) - \theta(-\omega - v_2 \Delta k_{2f}) \right], \quad (34)$$

Just like in the case of the tunneling current I_{tun}^B between two integer QHE edges, there are two threshold voltages, the positive threshold $\omega = v_3 \Delta k_{2f}$ and the negative one $\omega = -v_2 \Delta k_{2f}$. However, in contrast to I_{tun}^B , the tunneling current I_{tun}^A increases smoothly as the voltage passes the thresholds. At $\omega \gtrsim v_3 \Delta k_{2f}$, the tunneling current I_{tun}^A behaves as $\sim (\omega - v_3 \Delta k_{2f})^3$, and at $\omega \lesssim -v_2 \Delta k_{2f}$, $I_{\text{tun}}^A \sim -(\omega + v_2 \Delta k_{2f})^7$. Thus I_{tun}^A follows power laws near the thresholds. The exponents in the scaling laws for the current near the thresholds provide information about states. However, inter-edge Coulomb interactions may change these exponents and make them non-universal. When $|\omega| \gg v_2 \Delta k_{2f}$ and $v_3 \Delta k_{2f}$, I_{tun}^A will asymptotically behave like $\sim \omega^{10}$ for both positive and negative voltages. We plotted the differential conductance $G^A_{\text{tun}} = \partial I_{\text{tun}}^A / \partial \omega$ as a function of ω at fixed Δk_{2f} , and a function of Δk_{2f} at fixed ω in Fig. 5.

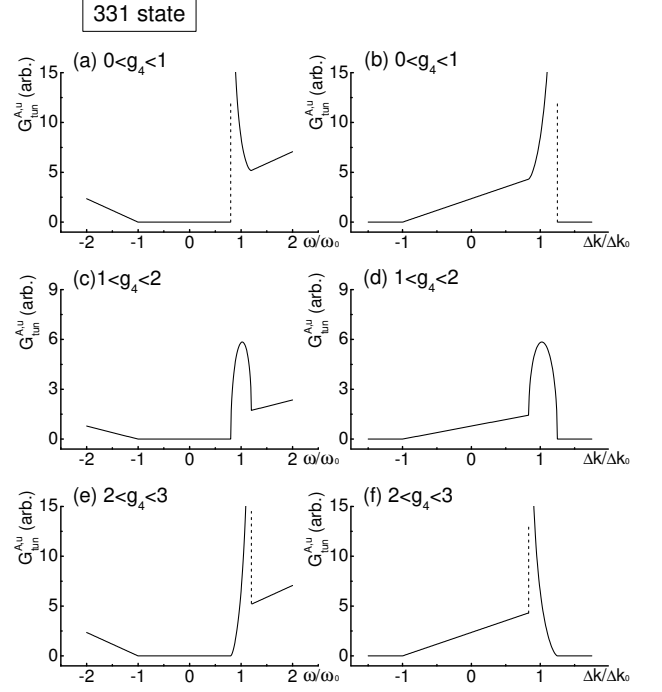


FIG. 6: Voltage and momentum mismatch dependence of the tunneling differential conductance $G^{A,u}_{\text{tun}}$ in the 331 state; u is either a or b . We have chosen the ratios of the edge velocities to be $v_3/v_2 = 0.8$ and $v_4/v_2 = 1.2$. The left three panels show the voltage dependence of $G^{A,u}_{\text{tun}}$ at a fixed momentum mismatch Δk for 3 cases of different scaling exponent ranges: (a) $0 < g_4 < 1$; (c) $1 < g_4 < 2$; (e) $2 < g_4 < 3$; we set $g_4 = 0.5, 1.5$ and 2.5 respectively in the plots. Voltage is shown in units of $\omega_0 = v_2 \Delta k$. Panels (b), (d) and (f) show the same three cases for the momentum mismatch dependence of $G^{A,u}_{\text{tun}}$ at a fixed ω with the momentum expressed in units of $\Delta k_0 = \omega/v_2$. The differential conductance is shown in arbitrary units.

B. 331 state

The 331 state⁷ has the edge Lagrangian density

$$\mathcal{L}_{\text{frac}} = -\frac{\hbar}{4\pi} (3\partial_t \phi_3 \partial_x \phi_3 - 2\partial_t \phi_3 \partial_x \phi_4 - 2\partial_t \phi_4 \partial_x \phi_3 + 4\partial_t \phi_4 \partial_x \phi_4 + \sum_{m,n=3,4} V_{mn} \partial_x \phi_m \partial_x \phi_n). \quad (35)$$

Both modes ϕ_3 and ϕ_4 are right-moving, and the real symmetric matrix V represents intra-edge interactions. There are two most relevant electron operators in this model, $\tilde{\Psi}_{\text{frac}}^a = e^{i3\phi_3 - i2\phi_4}$ and $\tilde{\Psi}_{\text{frac}}^b = e^{i\phi_3 + i2\phi_4}$. Before applying Eq. (24) to the calculation of the tunneling current, one needs to compute the correlation functions of $\tilde{\Psi}_{\text{frac}}^a$ and $\tilde{\Psi}_{\text{frac}}^b$. Since the Lagrangian density $\mathcal{L}_{\text{frac}}$ is quadratic, we can rewrite it in terms of two decoupled fields $\tilde{\phi}_3$ and $\tilde{\phi}_4$, such that

$$\mathcal{L}_{\text{frac}} = -\frac{\hbar}{4\pi} \sum_{n=3,4} \partial_x \tilde{\phi}_n (\partial_t + v_n \partial_x) \partial_x \tilde{\phi}_n. \quad (36)$$

$\tilde{\phi}_3$ and $\tilde{\phi}_4$ are linear combinations of ϕ_3 and ϕ_4 , with $\langle 0|\tilde{\phi}_n(x,t)\tilde{\phi}_n(0,0)|0\rangle = -\ln[\delta + i(t+x/v_n)]$, where the velocities are

$$v_{3,4} = \frac{1}{16} \left(4V_{33} + 4V_{34} + 3V_{44} \mp \sqrt{(1+x^2)} \times |4V_{33} + 4V_{34} - V_{44}| \right), \quad (37)$$

and $x = 2\sqrt{2}(V_{44} + 2V_{34})/(4V_{33} + 4V_{34} - V_{44})$ is an interaction parameter. Note that v_3 is smaller than v_4 . It is easy to prove that both v_3 and v_4 are positive, so $\tilde{\phi}_3$ and $\tilde{\phi}_4$ are right-moving. In the limit of strong interaction, $(V_{34})^2 \rightarrow V_{33}V_{44}$, v_3 approaches 0. The two-point correlation functions of those operators can be expressed as

$$\begin{aligned} \langle 0|\tilde{\Psi}_{\text{frac}}^{u\dagger}(x,t)\tilde{\Psi}_{\text{frac}}^u(0,0)|0\rangle \\ = \frac{1}{[\delta + i(t-x/v_3)]^{g_3^u}[\delta + i(t-x/v_4)]^{g_4^u}}, \end{aligned} \quad (38)$$

where $u = a, b$ and the scaling exponents

$$g_{3,4}^u = \frac{3}{2} \mp \frac{1 - \sigma_u 2\sqrt{2}x}{2\sqrt{1+x^2}} \text{sign}(4V_{33} + 4V_{34} - V_{44}); \quad (39)$$

the sign factors $\sigma_a = +1$, $\sigma_b = -1$. It is worth to notice that the sum of g_3^u and g_4^u is always 3.

There are two tunneling operators in the action. They are proportional to $\tilde{\Psi}_{\text{frac}}^a$ and $\tilde{\Psi}_{\text{frac}}^b$. These tunneling operators are responsible for two contributions to the current. Based on Eq.(38) and Eq. (24), both contributions have the form

$$\begin{aligned} I_{\text{tun}}^{A,u} = -L \frac{4\pi^2 e |\gamma_A|^2}{\hbar^2 \Gamma(g_3) \Gamma(g_4)} v_{24}^{g_4} v_{23}^{g_3} \left(\frac{\omega}{v_2} + \Delta k_{2f} \right)^2 \\ \times \begin{cases} B(1, g_4, g_3), & \omega > v_4 \Delta k_{2f} \\ B\left(\frac{v_{34}(\omega/v_3 - \Delta k_{2f})}{v_{24}(\omega/v_2 + \Delta k_{2f})}, g_4, g_3\right), & v_3 \Delta k_{2f} < \omega < v_4 \Delta k_{2f} \\ 0, & -v_2 \Delta k_{2f} < \omega < v_3 \Delta k_{2f} \\ -B(1, g_4, g_3), & \omega < -v_2 \Delta k_{2f}, \end{cases} \end{aligned} \quad (40)$$

where $u = a$ or b . We omitted the index u in the scaling exponents g_3 and g_4 , in the tunneling amplitude γ_A , and in the momentum mismatch Δk_{2f} in Eq. (40). $B(z, g_4, g_3)$ is the incomplete Beta function, and $v_{23} = v_2 v_3 / (v_2 + v_3)$, $v_{24} = v_2 v_4 / (v_2 + v_4)$ and $v_{34} = v_3 v_4 / (v_4 - v_3)$.

Consider any of the two contributions $I_{\text{tun}}^{A,a}$ or $I_{\text{tun}}^{A,b}$, Eq. (40). We see expected singularities marked by the edge velocities, with two singularities on the positive voltage side and one on the negative voltage side. The incomplete Beta function $B(z, g_4, g_3)$ has the following asymptotic behaviors

$$B(z, g_4, g_3) \sim \begin{cases} z^{g_4}, & z \sim 0 \\ (1-z)^{g_3} + \text{const.}, & z \sim 1 \end{cases} \quad (41)$$

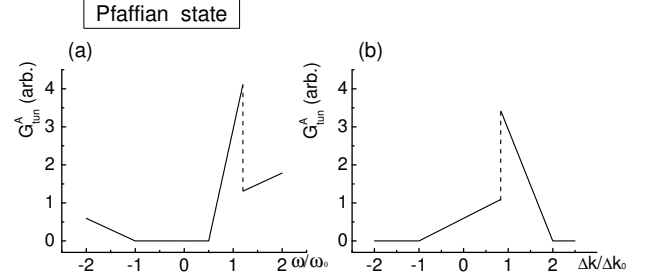


FIG. 7: (a) Voltage dependence of the tunneling differential conductance G_{tun}^A in the Pfaffian state. The reference voltage $\omega_0 = v_2 \Delta k$. (b) Momentum mismatch dependence of G_{tun}^A in the Pfaffian state. The reference momentum $\Delta k_0 = \omega/v_2$. We set the edge velocity ratios, $v_3/v_2 = 1.2$ and $v_\lambda/v_2 = 0.5$. G_{tun}^A is shown in arbitrary units.

Thus, when $\omega \gtrsim v_3 \Delta k_{2f}$, the differential conductance $G_{\text{tun}}^{A,u} \sim (\omega/v_3 - \Delta k_{2f})^{g_4-1}$, which is singular at $\omega = v_3 \Delta k_{2f}$, if $g_4 < 1$. Hence, the differential conductance diverges near the threshold. Similarly, $G_{\text{tun}}^{A,u}$ is singular at $\omega = v_4 \Delta k_{2f}$, if $g_3 < 1$, i.e., $g_4 > 2$. Hence, the shape of the $G_{\text{tun}}^{A,u} \sim \omega$ is quite different at different values of g_3 and g_4 , i.e., different interaction strengths x . Fig. 6 shows the dependence of $G_{\text{tun}}^{A,u}$ on ω and Δk_{2f} in 3 different cases: $g_4 < 1$, $1 < g_4 < 2$ and $g_4 > 2$. The total differential conductance $G_{\text{tun}}^A = G_{\text{tun}}^{A,a} + G_{\text{tun}}^{A,b}$ has two sets of singularities originating from the two individual contributions to the current. The shape of the curve of $G_{\text{tun}}^A(\omega)$ depends on the relative values of γ_A^a v.s. γ_A^b , Δk_{2f}^a v.s. Δk_{2f}^b , and g_4^a v.s. g_4^b . Thus, momentum-resolved tunneling allows one to extract considerable information about the details of the edge theory.

C. Pfaffian state

The Pfaffian state has the edge Lagrangian density²

$$\mathcal{L}_{\text{frac}} = -\frac{2\hbar}{4\pi} \partial_x \phi_3 (\partial_t + v_3 \partial_x) \phi_3 + i\lambda (\partial_t + v_\lambda \partial_x) \lambda \quad (42)$$

where ϕ_3 is the right-moving charged boson mode and λ is the neutral Majorana fermion mode. The most relevant electron operator is $\tilde{\Psi}_{\text{frac}} = \lambda \exp(i2\phi_3)$. Its correlation function $G = 1/[(\delta + i(t-x/v_3))^2 (\delta + i(t-x/v_\lambda))]$ equals the product of the correlation function of the Majorana fermion and the correlation function of the exponent of the Bose-field. The velocity of the charged mode exceeds the Majorana fermion velocity, $v_\lambda < v_3$. A straightforward application of the results of the previous section

yields the tunneling current

$$I_{\text{tun}}^A = -L \frac{2\pi^2 e |\gamma_A|^2}{\hbar^2} v_{2\lambda} \times \begin{cases} v_{23}^2 (\omega/v_2 + \Delta k_{2f})^2, & \omega > v_3 \Delta k_{2f} \\ v_{3\lambda}^2 (\omega/v_\lambda - \Delta k_{2f})^2, & v_\lambda \Delta k_{2f} < \omega < v_3 \Delta k_{2f} \\ 0, & -v_2 \Delta k_{2f} < \omega < v_\lambda \Delta k_{2f} \\ -v_{23}^2 (\omega/v_2 + \Delta k_{2f})^2, & \omega < -v_2 \Delta k_{2f} \end{cases} \quad (43)$$

where $v_{2\lambda} = v_\lambda v_2 / (v_2 + v_\lambda)$, $v_{23} = v_2 v_3 / (v_3 + v_2)$ and $v_{3\lambda} = v_3 v_\lambda / (v_3 - v_\lambda)$. Singularities appear again, two of them on the positive voltage side and one on the negative voltage side, quite similar to the results for the 331 state. However, the Pfaffian state can be distinguished from the 331 state by the appearance of a discontinuity for G_{tun}^A at $\omega = v_3 \Delta k$ (see Fig. 7). On the negative voltage side, G_{tun}^A behaves in the same way as in the 331 state, i.e., it is a linear function of ω .

D. Reconstructed Pfaffian state

The reconstructed Pfaffian state⁷ has the Lagrangian density

$$\mathcal{L}_{\text{frac}} = -\frac{\hbar}{4\pi} [2\partial_x \phi_c (\partial_t + v_c \partial_x) \phi_c + \partial_x \phi_n (\partial_t + v_n \partial_x) \phi_n + 2v_{nc} \partial \phi_c \phi_n] + i\lambda (\partial_t - v_\lambda \partial_x) \lambda, \quad (44)$$

where ϕ_c is a charged mode and ϕ_n is a neutral mode. There are three most relevant electron operators $\Psi_{\text{frac}}^\pm = \exp(i2\phi_c \pm \phi_n)$ and $\Psi_{\text{frac}}^\lambda = \lambda \exp(i2\phi_c)$. Thus, we need to consider three tunneling operators, proportional to these three electron operators. As discussed in the previous section they generate three independent contributions to the tunneling current I_{tun}^A . We first discuss the current contributions which originate from the tunneling terms containing Ψ_{frac}^\pm . For these two contributions, the situation is quite similar to the 331 state because the Majorana fermion does not enter the operators Ψ_{frac}^\pm . We diagonalize the bosonic part of the effective action (44) into the form of Eq. (36). This requires a transformation from the original fields $\{\phi_c, \phi_n\}$ to two free fields $\{\tilde{\phi}_3, \tilde{\phi}_4\}$ with velocities $\{v_3, v_4\}$ respectively. Then the two-point correlation function $\langle 0 | \Psi_{\text{frac}}^{\pm\dagger}(x, t) \Psi_{\text{frac}}^\pm(0, 0) | 0 \rangle$ can be calculated as we did for 331 state. With Eq. (24) we then obtain the same form of the tunneling current $I_{\text{tun}}^{A,\pm}$ as in Eq. (40), but with different tunneling amplitudes, momentum mismatches, edge velocities and scaling exponents. The edge velocities are

$$v_{3,4} = \frac{1}{2} (v_c + v_n \mp (v_c - v_n) \sqrt{1 + 2x^2}), \quad (45)$$

and scaling exponents are

$$g_{3,4}^\sigma = \frac{3}{2} \mp \frac{1 + 4\sigma x}{2\sqrt{1 + 2x^2}}, \quad (46)$$

where $\sigma = +1$ for the case of Ψ_{frac}^+ and $\sigma = -1$ for Ψ_{frac}^- ; the interaction parameter $x = v_{nc}/(v_c - v_n)$. It is assumed that $(v_c - v_n)$ is positive. Indeed, we expect the charged mode to be faster than the neutral mode. Thus, for repulsive interactions x is always positive. Similar to the 331 state, different values of x give significantly different shapes of the $G_{\text{tun}}^{A,\pm}$ curve, i.e., divergence may appear for certain values of x . All three cases discussed in the subsection on the 331 state could also emerge in the edge reconstructed Pfaffian state.

Now let us turn to the tunneling operator, proportional to $\Psi_{\text{frac}}^\lambda$. In this case all four modes participate in the tunneling process. The correlation function of the field $\Psi_{\text{frac}}^\lambda$ is the product of the correlation function of two Majorana fermions and the Bose part. The correlation function for Majorana fermions is the same as for ordinary fermions, $1/[\delta + i(t + x/v_\lambda)]$. The Bose part has the same structure as in Eq. (38) with the scaling exponents

$$g_{3,4}^\lambda = 1 \mp \frac{1}{\sqrt{1 + 2x^2}}, \quad (47)$$

where different signs correspond to indices 3 and 4. Again, by using Eq. (24) we obtain the following contribution to the tunneling current:

$$I_{\text{tun}}^{A,\lambda} = -L \frac{4\pi^2 e |\gamma_A^\lambda|^2}{\hbar^2 \Gamma(g_3 + 1) \Gamma(g_4)} v_{2\lambda} \text{sign}(\omega) \times \left[v_{3\lambda}^{g_3} v_{4\lambda}^{g_4} \left(\frac{\omega}{v_\lambda} + \Delta k_{2f}^\lambda \right)^2 B(f(\omega), g_4, g_3 + 1) - v_{23}^{g_3} v_{24}^{g_4} \left(\frac{\omega}{v_2} + \Delta k_{2f}^\lambda \right)^2 B(g(\omega), g_4, g_3 + 1) \right], \quad (48)$$

where

$$f(\omega) = \begin{cases} \frac{(\omega/v_3 - \Delta k_{2f}^\lambda) v_{34}}{(\omega/v_\lambda + \Delta k_{2f}^\lambda) v_{4\lambda}}, & v_3 < \frac{\omega}{\Delta k_{2f}^\lambda} < v_4 \\ 1, & \frac{\omega}{\Delta k_{2f}^\lambda} < -v_\lambda \text{ or } > v_4 \\ 0, & -v_\lambda < \frac{\omega}{\Delta k_{2f}^\lambda} < v_3 \end{cases} \quad (49)$$

and

$$g(\omega) = \begin{cases} \frac{(\omega/v_3 - \Delta k_{2f}^\lambda) v_{34}}{(\omega/v_2 + \Delta k_{2f}^\lambda) v_{24}}, & v_3 < \frac{\omega}{\Delta k_{2f}^\lambda} < v_4 \\ 1, & \frac{\omega}{\Delta k_{2f}^\lambda} < -v_2 \text{ or } > v_4 \\ 0, & -v_2 < \frac{\omega}{\Delta k_{2f}^\lambda} < v_3 \end{cases} \quad (50)$$

The dependence of $G_{\text{tun}}^{A,\lambda}$ on the voltage ω and momentum mismatch Δk_{2f}^λ is illustrated in Fig. 8. There are no divergencies for any g_4^λ . All singularities appear as voltage thresholds or discontinuities of the derivative of $G_{\text{tun}}^\lambda(\omega)$. The Majorana fermion mode is responsible for the negative voltage threshold (we assume that the Majorana is slower than the integer QHE mode at the opposite side of the junction; the assumption is reasonable as the integer QHE mode is charged).

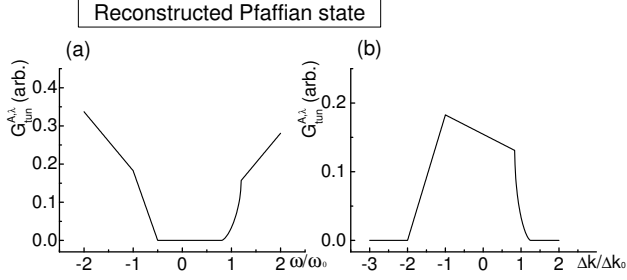


FIG. 8: The differential conductance $G_{\text{tun}}^{A,\lambda}$ in the edge reconstructed Pfaffian state. Panels (a) and (b) show the voltage and momentum mismatch dependence of $G_{\text{tun}}^{A,\lambda}$ (in arbitrary units) respectively. The reference voltage $\omega_0 = v_2 \Delta k$ and the reference momentum mismatch $\Delta k_0 = \omega/v_2$. We have set $v_\lambda/v_2 = 0.5$, $v_3/v_2 = 0.8$, $v_4/v_2 = 1.2$ and the scaling exponent $g_4 = 1.5$

Thus, in the edge reconstructed Pfaffian state, three sets of singularities can be observed. Each set corresponds to one of the three most relevant electron operators. One set contains more singularities than the other two. That extra singularity is due to the neutral Majorana fermion mode.

E. Disorder-dominated anti-Pfaffian state

The very name of this state shows that the momentum-resolved tunneling can only have limited utility in this case. Indeed, momentum conservation assumes that disorder can be neglected and this assumption fails for the state under consideration^{5,6}. In the disorder-dominated anti-Pfaffian state, the amplitudes of the electron tunneling operators are expected to be random. Thus, one expects that interference between different tunneling sites is irrelevant for the total tunneling current since the disorder average of the product of two tunneling amplitudes from two different points is zero. Hence, the leading contribution to the current is the same as for the tunneling through a single quantum point contact. Nevertheless, momentum resolved tunneling might be possible for electron pairs. This happens, if disorder only couples to neutral modes and does not affect the charged mode. As we see below, the momentum resolved tunneling current of pairs is the same as for the $K = 8$ state.

In the disorder-dominated anti-Pfaffian edge state, there are 3 left-moving $SO(3)$ -symmetric Majorana modes and one right moving charged mode, with the Lagrangian density^{5,6}

$$\mathcal{L}_{\text{frac}} = -\frac{2\hbar}{4\pi} \partial_x \phi_c (\partial_t + v_c \partial_x) \phi_c + i \sum_n^3 [\lambda_n (\partial_t - v_\lambda \partial_x) \lambda_n]. \quad (51)$$

There are three electron operators corresponding to the three Majorana fermions, $\Psi_{\text{frac}}^n = \lambda_n e^{i\phi_c}$, $n = 1, 2, 3$. Their products yield pair operators. We focus on the pair

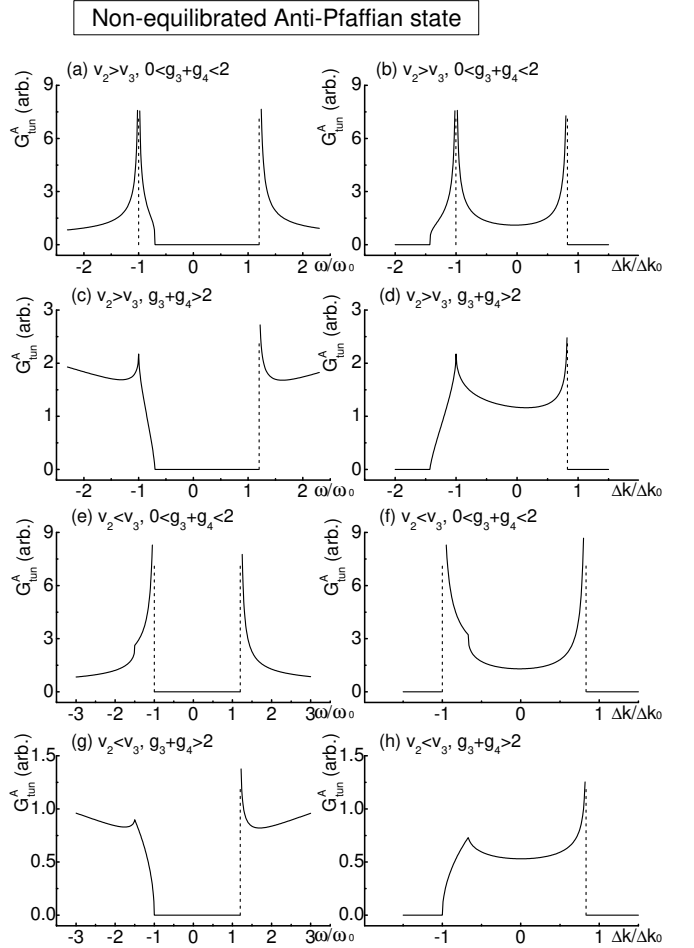


FIG. 9: Differential conductance G_{tun}^A in the non-equilibrated anti-Pfaffian edge state. All left panels show the voltage dependence of G_{tun}^A and right panels show the momentum mismatch dependence of G_{tun}^A , at different choices of v_3/v_2 and $g_3 + g_4$. In the top four panels, we have chosen $v_3/v_2 = 0.7$, and in the bottom four panels $v_3/v_2 = 1.5$. $v_4/v_2 = 1.2$ for all cases. In panels (a), (b), (e) and (f), illustrating the $0 < g_3 + g_4 < 2$ cases, we set $g_3 + g_4 = 1.5$. In panels (c), (d), (g) and (h), illustrating the $g_3 + g_4 > 2$ cases, we set $g_3 + g_4 = 2.5$. The reference voltage $\omega_0 = v_2 \Delta k$ and the reference momentum mismatch $\Delta k_0 = \omega/v_2$. G_{tun}^A is shown in arbitrary units.

operator $\exp(2i\phi_c)$ which contains no information about neutral modes. One can easily verify that its correlation function is the same as the correlation function of the pair operator in the $K = 8$ state. Hence, all results can be taken without modifications from our discussion of the $K = 8$ state. Certainly, the total tunneling current includes also a single-electron part. One may expect that it is greater than the momentum-resolved contribution due to the pair tunneling since the tunneling amplitude is greater for single electrons than for pairs.

F. Non-equilibrated anti-Pfaffian state

The non-equilibrated anti-Pfaffian edge has the Lagrangian density⁶

$$\begin{aligned}\mathcal{L}_{\text{frac}} = & -\frac{\hbar}{4\pi}[\partial_x\phi_{c1}(\partial_t + v_{c1}\partial_x)\phi_{c1} \\ & + 2\partial_x\phi_{c2}(-\partial_t + v_{c2}\partial_x)\phi_{c2} + 2v_{12}\partial_x\phi_{c1}\partial_x\phi_{c2}] \\ & + i\lambda(\partial_t - v_\lambda\partial_x)\lambda.\end{aligned}\quad (52)$$

Again the action can be rewritten in terms of two linear combinations of the Bose fields ϕ_{c1} and ϕ_{c2} : a free left-moving mode $\tilde{\phi}_3$ and a right-moving mode $\tilde{\phi}_4$ with

$$\begin{aligned}I_{\text{tun}}^A = & -L\frac{4\pi^2e|\gamma_A|^2}{\hbar^2\Gamma(g_3)\Gamma(g_4)}v_{34}^{g_3+g_4-1}\text{sign}(\omega) \\ & \times \begin{cases} \frac{v_{24}}{g_3}\left|\frac{\omega}{v_4} - \Delta k_{2f}\right|^{g_3}\left|\frac{\omega}{v_3} + \Delta k_{2f}\right|^{g_4-1}F(1, 1-g_4, 1+g_3, \frac{v_{24}(\omega/v_4 - \Delta k_{2f})}{v_{23}(\omega/v_3 + \Delta k_{2f})}), & \omega > v_4\Delta k_{2f} \text{ or } \omega < -v_2\Delta k_{2f} \\ \frac{v_{23}}{g_4}\left|\frac{\omega}{v_4} - \Delta k_{2f}\right|^{g_3-1}\left|\frac{\omega}{v_3} + \Delta k_{2f}\right|^{g_4}F(1, 1-g_3, 1+g_4, \frac{v_{23}(\omega/v_3 + \Delta k_{2f})}{v_{24}(\omega/v_4 - \Delta k_{2f})}), & -v_2\Delta k_{2f} < \omega < -v_3\Delta k_{2f} \\ 0, & \text{otherwise} \end{cases}\end{aligned}\quad (53)$$

where the scaling exponents equal

$$g_{3,4} = \frac{1}{2\sqrt{1-2x^2}} \mp \frac{1}{2} \quad (54)$$

and F is the hypergeometric function.

For the interaction strength we focus on, $0 < x < 2/3$, we always have $0 < g_3 < 1$ and $1 < g_4 < 2$. Asymptotically, $I_{\text{tun}}^A \sim (\omega - v_4\Delta k_{2f})^{g_3}$ when $\omega \gtrsim v_4\Delta k_{2f}$. Thus, $\omega = v_4\Delta k_{2f}$ corresponds to a divergency of the differential conductance. If $\omega \lesssim -v_3\Delta k_{2f}$ then the tunneling current is asymptotically equal to $(\omega + v_3\Delta k_{2f})^{g_4}$. When $\omega \approx -v_2\Delta k_{2f}$, we have $I_{\text{tun}}^A \sim (\omega + v_2\Delta k_{2f})^{g_3+g_4-1}$. Hence, when $g_3 + g_4 < 2$, the differential conductance diverges at $-v_2\Delta k_{2f}$, while for $g_3 + g_4 > 2$ only a cusp is present as is shown in Fig. 9.

If $v_2 < v_3$ then the tunneling current is

$$\begin{aligned}I_{\text{tun}}^A = & -L\frac{4\pi^2e|\gamma|^2}{\hbar^2\Gamma(g_3)\Gamma(g_4)}v_{23}^{g_3}v_{24}^{g_4}\left|\frac{\omega}{v_2} + \Delta k_{2f}\right|^{g_3+g_4-1}\text{sign}(\omega) \\ & \times \begin{cases} B(\frac{v_{34}(\omega/v_4 - \Delta k_{2f})}{v_{23}(\omega/v_2 + \Delta k_{2f})}, g_3, g_4), & \frac{\omega}{\Delta k_{2f}} > v_4 \text{ or } < -v_3 \\ B(1, g_3, g_4), & -v_3 < \frac{\omega}{\Delta k_{2f}} < -v_2 \\ 0, & \text{otherwise} \end{cases}\end{aligned}\quad (55)$$

In this case the behavior near $\omega = v_4\Delta k_{2f}$ is the same as above. The behavior near $\omega = -v_3\Delta k_{2f}$ and $\omega = -v_2\Delta k_{2f}$ is also the same as above but these singularities appear now in the opposite order since $v_2 < v_3$. The differential conductance is shown in Fig. 9.

velocities v_3 and v_4 respectively. From the renormalization group, we find that the most relevant electron operators depend on the interaction strength parameter $x = v_{12}/(v_{c1} + v_{c2})$. Below we will only consider $x < 2/3$. The action (52) is only stable for $x < 1/\sqrt{2}$ and hence we ignore a small region $2/3 < x < 1/\sqrt{2}$ in the parameter space. For $x < 2/3$, the most relevant electron operator is $\Psi_{\text{frac}} = e^{i\phi_{c1}}$.

The expression for the tunneling current I_{tun}^A and, in particular, the asymptotic behavior near singularities depends on the relative values of v_2 and v_3 , the velocities of the two left-moving modes. If $v_2 > v_3$ we obtain the following tunneling current

VI. DISCUSSION

In experiments, only the total tunneling current

$$I_{\text{tun}} = \sum_i I_{\text{tun}}^{A,i} + I_{\text{tun}}^B + I_{\text{tun}}^C \quad (56)$$

and the total tunneling differential conductance G_{tun} can be measured, thus, singularities originating from all three contributions to the current will be seen. However, the last two contributions to the current (56) always exhibit the same behavior. Singularities in the voltage dependence of the differential conductance, originating from the first contribution to the tunneling current, are summarized in Table I except for the disorder dominated anti-Pfaffian state. A closely related behavior can be obtained in the experiment with tunneling into a quantum wire at a fixed low voltage. In that experiment the dependence of the conductance on the Fermi momentum in the quantum wire can be probed. The Fermi momentum can be controlled by a gate voltage. Singularities in the Fermi momentum dependence of the differential conductance are similar to those in the voltage dependence of the differential conductance, as seen from Figs. 5-9.

Finally, we briefly discuss tunneling between two identical $\nu = 5/2$ states. A significant difference from the previous discussion comes from the symmetry of the system. The symmetry considerations yield the identity $I_{\text{tun}}(\omega) = -I_{\text{tun}}(-\omega)$. In contrast to our previous discussion, it is no longer possible to read the propagation

TABLE I: Summary of singularities in the voltage dependence of the differential conductance G_{tun}^A for different $5/2$ states. The “Modes” column shows the numbers of left- and right-moving modes in the fractional edge, the number in the brackets being the number of Majorana modes. “A” or “N” in the next column means Abelian or non-Abelian statistics. The “Singularities” shows the number of singularities, including divergencies (S), discontinuities (D) and cusps (C), i.e., discontinuities of the first or higher derivative of the voltage dependence of G_{tun}^A .

State	Modes	Statistics	Singularities
K=8	1R	A	2C
331	2R	A	4C+2S or 5C+S
Pfaffian	2R(1)	N	2C+D
Edge-reconstructed Pfaffian	1L(1) + 2R	N	8C+2S or 9C+S
Non-equilibrated anti-Pfaffian	2L(1) + 1R	N	C+2S or 2C+S

direction of the modes from the $I - V$ curve as there is no difference between positive and negative voltages.

The tunneling current through a line junction between two $5/2$ states expresses as

$$I_{\text{tun}} = I_{\text{tun}}^A(\Delta k, \omega) + I_{\text{tun}}^A(-\Delta k, \omega) + I_{\text{tun}}^B + I_{\text{tun}}^C + I_{\text{tun}}^F, \quad (57)$$

where I_{tun}^F is the tunneling current between two fractional QHE edges, I_{tun}^A stays for tunneling between integer QHE modes on one side of the junction and fractional QHE modes on the other side of the junction, and $I_{\text{tun}}^{B,C}$ describe tunneling between integer QHE modes on different sides of the junction. Since the tunneling operator between two fractional edge modes is less relevant than the other tunneling operators, the contribution I_{tun}^F is smaller than the other contributions. All remaining contributions have already been calculated above.

In conclusion, we considered the electron tunneling into $\nu = 5/2$ QHE states through a line junction. Momentum resolved tunneling can distinguish six proposed candidate states. The number of singularities in the $I - V$ curve gives the number of the modes on two sides of the

junction. The nature and propagation directions of the modes can be read from the details of the $I - V$ curve.

Acknowledgments

We would like to thank Y. Gefen, M. Grayson, M. Heiblum and F. Li for valuable discussions. CW thanks Weizmann Institute of Science for hospitality. This work was supported by the NSF under Grant No. DMR-0544116 and BSF under Grand No. 2006371.

Note added. When this paper was being finalized we learned about a preprint³⁷ which considers momentum-resolved tunneling into a $5/2$ edge in a different geometry. In contrast to our paper, Ref. 37 only considers two candidate states: Pfaffian and nonequilibrated anti-Pfaffian. As discussed above, nonequilibrated anti-Pfaffian state can be probed with a conductance measurement in a bar geometry since its conductance is $7e^2/(2h)$ in contrast to other candidate states. In this paper, we show how the Pfaffian state can be distinguished from several other proposed states which have the same conductance in the bar geometry.

-
- ¹ R. E. Prange and S. M. Girvin, eds., *The Quantum Hall Effect* (Springer-Verlag, New York, 1987).
 - ² C. Nayak, S. H. Simon, A. Stern, M. Freedman, and S. D. Sarma, Rev. Mod. Phys. **80**, 1083 (2008).
 - ³ A. Y. Kitaev, Ann. Phys. **330**, 2 (2003).
 - ⁴ G. Moore and N. Reed, Nucl. Phys. B **360**, 362 (1991).
 - ⁵ S.-S. Lee, S. Ryu, C. Nayak, and M. P. A. Fisher, Phys. Rev. Lett. **99**, 236807 (2007).
 - ⁶ M. Levin, B. I. Halperin, and B. Rosenow, Phys. Rev. Lett. **99**, 236806 (2007).
 - ⁷ B. J. Overbosch and X.-G. Wen (2008), arXiv:0804.2087 (unpublished).
 - ⁸ X.-G. Wen and A. Zee, Phys. Rev. B **46**, 2290 (1992).
 - ⁹ M. Dolev, M. Heiblum, V. Umansky, A. Stern, and D. Mahalu, Nature **452**, 829 (2008).
 - ¹⁰ I. P. Radu, J. B. Miller, C. M. Marcus, M. A. Kastner, L. N. Pfeiffer, and K. W. West, Science **320**, 899 (2008).
 - ¹¹ R. L. Willett, L. N. Pfeiffer, and K. W. West, PNAS **106**,

- 8853 (2009).
- ¹² C. de C. Chamon, D. E. Freed, S. A. Kivelson, S. L. Sondhi, and X. G. Wen, Phys. Rev. B **55**, 2331 (1997).
- ¹³ E. Fradkin, C. Nayak, A. Tsvelik, and F. Wilczek, Nucl. Phys. B **516**, 704 (1998).
- ¹⁴ S. Das Sarma, M. Freedman, and C. Nayak, Phys. Rev. Lett. **94**, 166802 (2005).
- ¹⁵ A. Stern and B. I. Halperin, Phys. Rev. Lett. **96**, 016802 (2006).
- ¹⁶ P. Bonderson, A. Kitaev, and K. Shtengel, Phys. Rev. Lett. **96**, 016803 (2006).
- ¹⁷ C. L. Kane, Phys. Rev. Lett. **90**, 226802 (2003).
- ¹⁸ Y. Ji, Y. C. Chung, D. Sprinzak, M. Heiblum, and D. M. and H. Shtrikman, Nature **422**, 415 (2003).
- ¹⁹ K. T. Law, D. E. Feldman, and Y. Gefen, Phys. Rev. B **74**, 045319 (2006).
- ²⁰ D. E. Feldman and A. Kitaev, Phys. Rev. Lett. **97**, 186803 (2006).

- ²¹ D. E. Feldman, Y. Gefen, A. Kitaev, K. T. Law, and A. Stern, Phys. Rev. B **76**, 085333 (2007).
- ²² K. T. Law, Phys. Rev. B **77**, 205310 (2008).
- ²³ A. M. Chang, Rev. Mod. Phys. **75**, 1449 (2003).
- ²⁴ D. E. Feldman and F. Li, Phys. Rev. B **78**, 161304 (2008).
- ²⁵ B. J. Overbosch and C. Chamon, Phys. Rev. B **80**, 035319 (2009).
- ²⁶ W. Kang, H. Stormer, L. Pfeiffer, K. Baldwin, and K. West, Nature **403**, 59 (2000).
- ²⁷ U. Zülicke and E. Shimshoni, Phys. Rev. Lett. **90**, 026802 (2003).
- ²⁸ A. Melikidze and K. Yang, Phys. Rev. B **70**, 161312 (2004).
- ²⁹ F. D. M. Haldane and E. H. Rezayi, Phys. Rev. Lett. **60**, 956 (1988).
- ³⁰ R. H. Morf, Phys. Rev. Lett. **80**, 1505 (1998).
- ³¹ E. H. Rezayi and F. D. M. Haldane, Phys. Rev. Lett. **84**, 4685 (2000).
- ³² X.-G. Wen, Int. J. Mod. Phys. B **6**, 1711 (1992).
- ³³ S. M. Girvin, Phys. Rev. B **29**, 6012 (1984).
- ³⁴ M. Huber, M. Grayson, M. Rother, R. Deutschmann, W. Biberacher, W. Wegscheider, M. Bichler, and G. Abstreiter, Physica E (Amsterdam) **12**, 125 (2002).
- ³⁵ X.-G. Wen, *Quantum Field Theory of Many-Body-System* (Oxford University Press, 2004).
- ³⁶ D. E. Feldman and Y. Gefen, Phys. Rev. B **67**, 115337 (2003).
- ³⁷ A. Seidel and K. Yang (2009), arXiv:0908.1970 (unpublished).